Carbohydrate Polymers 89 (2012) 632–639

Contents lists available at SciVerse ScienceDirect

Carbohydrate Polymers

journal homepage: www.elsevier.com/locate/carbpol

Nano-hybrid carboxymethyl-hexanoyl chitosan modified with (3-aminopropyl)triethoxysilane for camptothecin delivery

Meng-Hsuan Hsiao [1], Tsan-Hua Tung [1], Chi-Sheng Hsiao, Dean-Mo Liu *

Department of Materials Sciences and Engineering, National Chiao Tung University, 1001 Ta-hsueh Road, Hsinchu 300, Taiwan

ARTICLE INFO

Article history:
Received 19 February 2012
Received in revised form 19 March 2012
Accepted 21 March 2012
Available online 30 March 2012

Keywords:
Chitosan
Silane
Amphiphiles
Self-assembly
Drug delivery systems

ABSTRACT

Silane-modified amphiphilic chitosan was synthesized by anchoring a silane coupling agent, (3-aminopropyl)triethoxysilane, to a novel amphiphilic carboxymethyl-hexanoyl chitosan (CHC). The chemical structure of this new organic–inorganic hybrid molecule was characterized by FTIR and ^{13}C-, ^{29}Si-nuclear magnetic resonance, while the structural evolution was examined using scanning electron microscopy (SEM), transmission electron microscopy (TEM), X-ray diffraction (XRD), and dynamic light scattering (DLS). Experimental results indicated a self-assembly behaviour of molecules into nanoparticles with a stable polygonal geometry, consisting of ordered silane layers of 6 nm in thickness. The self-assembly property was found to be influenced by chemical composition and concentration of silane incorporated, while the size can be varied by the amount of anchored silane. It was also demonstrated that such vesicle exhibited excellent cytocompatibility and cellular internalization capability in ARPE-19 cell line, and presented well-controlled encapsulation and release profiles for (S)-(+)-camptothecin. These unique properties render it as a potential drug delivery nanosystem.

1. Introduction

Many approaches for the preparation of hybrid compounds have been recently reported. Among them, the synthesis of composites through the combination of polysaccharides and silicon-based materials has been widely reported for various fields, such as enzyme immobilization, porous materials and electrochemical sensors (Gamys, Beyou, & Bourgeat-Lam, 2010; Guo, Zheng, & Hu, 2008; Lei et al., 2011; Mullner, Schallon, Walther, Freitag, & Muller, 2010; Murakami et al., 2010; Qi et al., 2010; Salmah, Faisal, & Kamarudin, 2011; Tripathi & Shahi, 2008; Wang & Zhang, 2006; Yavuz et al., 2009). Furthermore, chitosan-based materials have been proposed for a range of biomedical applications (Hu, Liu, Du, & Yuan, 2009; Jayakumar et al., 2010; Liu, Chen, Liu, & Liu, 2008; Murakami et al., 2010; Muzzarelli, 1993, 2009; Wang & Zhang, 2006). Among those relevant reports, chitosan-based organic–inorganic hybrid molecules capable of self-assembling into well-organized architecture are rarely found. It is currently an important research objective to integrate diverse functions into a given nanoobject for advanced applications. This is particularly interesting in the area of biomedical and pharmaceutical industries. It would be highly desirable to take advantage of the biocompatibility of natural polymers, e.g., chitosan or its modified analogues, and combine this with the unique functions of inorganic components.

Nanostructures of pristine chitosan or its composite analogues have been widely reported for drug delivery practice, and a number of cross-linking agents have been proposed in order to stabilize the resulting nanoobjects upon dilution, for instance when administrated to the blood circulatory system. However, for most polymeric drug delivery nanoparticles reported in literature, burst release of drug has been frequently observed in the early-phase of the drug release, mainly due to swelling of the polymer and release of surface bound drug. This effect is even more pronounced for water-soluble polymers and most natural polymers. Thus, it is not unusual that polymeric drug nanocarriers suffer from uncontrollable loss or leakage upon delivery, making a final therapeutic dose practically un-predictable. Moreover, many water-soluble natural polymers exert less preference to encapsulate water-insoluble drugs, albeit some emulsification technologies or analogous skills have been developed to overcome the problem. It is highly desirable to modify a natural macromolecule, making it capable of undergoing self-assembly to effectively entrap water-insoluble drugs for subsequent controlled drug release while retaining the good biocompatibility of the template macromolecule.

Our earlier work has demonstrated a successful synthesis of a new type of chitosan, namely carboxymethyl-hexanoyl chitosan (CHC) (Liu et al., 2008), wherein the pristine chitosan was modified first by carboxymethylation, to increase the flexibility

* Corresponding author. Tel.: +886 3 571 2121x55391; fax: +886 3 572 4727.
E-mail address: deanmo_liu@yahoo.ca (D.-M. Liu).
[1] Equal contribution as first author.

0144-8617/$ – see front matter © 2012 Elsevier Ltd. All rights reserved.
http://dx.doi.org/10.1016/j.carbpol.2012.03.066

of chitosan molecular chains in water, followed by hydrophobic modification with hexanoyl groups, to create the resulting amphiphilic molecules. However, extensive swelling of the resulting CHC in aqueous solution caused early-phase burst release, the same scenario being observed in many chitosan-based drug carriers. Furthermore, the CHC molecules demonstrated encapsulation efficiencies for doxorubicin of about 50%, leaving room for improvement. Therefore, it was considered interesting to design an organic–inorganic hybrid molecule. The resulting hybrid molecule should be capable of self-assembly, have reduced swelling and improved optimal drug loading capacity. Most importantly, the inorganic component should assemble into dense shell-like structures with low permeability, which should provide sustained release as well as reduced burst release.

Here we report the synthesis of a hybrid organic–inorganic molecule through the use of the CHC chitosan as a starting organic matrix, which is further chemically modified using a coupling agent, (3-aminopropyl)triethoxysilane (APTES) to provide the inorganic component (silane).

2. Experimental

2.1. Materials

Chitosan (Mw = 215,000 g/mol, deacetylation degree = 85–90%) was purchased from Aldrich–Sigma. 2-Propanol, sodium hydroxide, chloroacetic acid, and hexanoyl anhydride were supplied from Sigma Co. (3-Aminopropyl)triethoxysilane (APTES) (purity > 98%) was bought from Fluka. 1-Ethyl-3-(3-dimethylaminopropyl) carbodiimide methiodide (EDC) and dialysis tubing cellulose membrane (Mw cut-off 12,400 g/mol, average flat width 33 mm) were purchased from Sigma–Aldrich.

2.2. Synthesis of silane–CHC hybrid macromolecules

Synthesis of carboxymethyl-hexanoyl chitosan, CHC, was successfully performed as previously described (Liu et al., 2008). The resulting amphiphilic CHC was further chemically modified with the incorporation of silane precursor. A small amount, 0.25 g, of CHC was dissolved and dispersed in 50 mL of water (0.5 wt%) under vigorous agitation at room temperature for 24 h until the CHC was fully dissolved. Subsequently, APTES was added into the CHC solution to achieve desired NH_2 of APTES to COOH of CHC (calculated) ratios, the nomenclature of APTES containing samples here forth used is CXA, where X is the NH_2:COOH ratio. Finally, 0.012 g of EDC was added as a catalyst (Murakami et al., 2010) and the mixture was gently stirred. The reaction was allowed to proceed for 24 h under a N_2 atmosphere to ensure a well-defined reaction environment (Wen & Wilkes, 1996). The resulting product was collected using a dialysis membrane in ethanol/water solution (75%, v/v) for 24 h followed by dialysis in pure ethanol for 24 h. The resulting powder, with white-yellow appearance, was obtained after evaporation and drying overnight in an oven at 50 °C.

2.3. Characterization

The chemical structure of the hybrid molecules was characterized by nuclear magnetic resonance (NMR) and Fourier transform infrared spectroscopy (FT-IR). ^{13}C and ^{29}Si solid-state NMR spectra were recorded at 79.49 and 100.62 MHz, on a (9.4 T) Bruker DSX400 WB NMR spectrometer. The FT-IR spectra of samples in KBr pellets were recorded (32 scans with a resolution of 4 cm^{-1}) on a Unican Mattson Mod 7000 FTIR. The structural morphology of the hybrid nanoparticles was analysed using scanning electron microscopy (SEM) (S 6500, JEOL2100, Japan) and transmission electron microscopy (TEM) (JEOL2100, Japan). The mean size and size distribution of the nanocapsules were measured by dynamic light scattering (BI-200SM Goniometer DLS, Brookhaven Inc., Holtsville, NY).

2.4. Self-assembly behaviour of silane–CHC hybrid

Pyrene has been frequently chosen as a fluorescence probe to monitor the self-aggregation behaviour of surfactants and polymers because of its high chemical affinity to hydrophobic microdomains. Pyrene emission spectra were obtained using a fluorescence spectrophotometer (Hitachi FL-4500, Japan). The probe was excited at 343 nm, and the emission spectra were recorded in the range of 350–500 nm at an integration time of 1.0 s. The excitation and emission slit openings were 10 nm.

2.5. Drug loading and release

The anti-cancer drug, (S)-(+)-camptothecin (CPT), was used as a model molecule to evaluate the drug release behaviour from the silane–CHC hybrid nanoparticles. The CPT-loaded hybrid nanoparticles were prepared by the following procedures. Briefly, 20 mg of CPT was fully dissolved in 5 mL DMSO, diluted to form 1000 μg/mL of CPT/DMSO solution, and then mixed with DI water (0.5/9.5, v/v) to obtain a final concentration of 50 μg/mL. The final solution mixture was stirred at room temperature for 30 min until a homogeneous appearance was visually observed. The different concentrations of silane–CHC hybrid molecules (0.5–9 mg/ml) were then added into the solution with a concentration of 2 mg/ml, the sample was kept under stirring at ambient temperature for 1 day before drug loading and release analyses. After stirring for 24 h, the samples were then separated from the aqueous solution by centrifugation at 8000 rpm and 20 °C for 20 min and analysed by ultraviolet absorption (UV) (SP-8001, Metertech Inc., Taiwan) at wavelength of 366 nm. The drug encapsulated efficiency (EE) can be obtained using the following equation:

$$EE = \frac{A - B}{A} \times 100\%$$

where A is the total amount of the CPT and B is the amount of CPT remaining in the supernatant.

The drug release behaviour from the hybrid nanoparticles was measured in a 5 mL PBS solution (pH 7.4) under the room temperature (25 °C). To measure the concentration of the drug in the PBS medium for a given period of time, the test tubes were subjected to centrifugation at 6000 rpm. A clear supernatant was separated and used to estimate the concentration of drug via the UV spectroscopic analysis. The remaining residue in the bottom of the test tubes was refreshed using 5 mL PBS medium, and the procedure of the centrifugation and UV analysis was repeated over a regular period of time to monitor the CPT release kinetics till no sign of release was observed. Each data was obtained in triplicate measurements.

2.6. Cell cytotoxicity and uptake

ARPE-19 (human retinal pigmented epithelium, derived from BCRC; BCRC number: 60383) cells were cultured in a medium of 90% 1:1 mixture of Dulbecco's modified Eagle's medium and Ham's F medium containing 1.2 g/L sodium bicarbonate, 2.5 mM L-glutamine, 15 mM HEPES and 0.5 mM sodium pyruvate; 10% foetal bovine serum. Cells were cultured in the complete medium at 37 °C in a humidified atmosphere of 5% CO_2 in air. For all experiments, cells were harvested from sub-confluent cultures by the use of trypsin and were re-suspended in fresh complete medium before plating. In vitro cytotoxicity of the hybrid nanoparticles with different silane/CHC ratios was examined using ARPE-19 cell line. Briefly, 1×10^4 cells were plated in 96-well plates to allow the cells to

attach and were then exposed to a serial concentration of the hybrid nanoparticles at 37 °C in an atmosphere with 5% CO_2. After 1 or 2 days of incubation, 20 μL of MTT solution was added and incubated for another 4 h. The medium was replaced with 200 μL of DMSO and the absorbance was monitored using a Sunrise absorbance microplate reader at dual wavelengths of 570 and 650 nm.

The cellular uptake of the hybrid nanoparticles was estimated using a fluorescein isothiocyanate (FITC) as the green-emitting fluorescein dye, attaching to the hybrid nanoparticles. The FITC-hybrid nanoparticles were incubated with the cells for different time durations and then studied by confocal microscopy (1000× magnification) (Nikon ECLIPSE TE2000-U, Japan).

3. Results and discussion

3.1. Infrared analysis

The hybrid molecules were prepared through the carbodiimide coupling reaction, where the carboxylic groups from the carboxymethyl ligands of the CHC chemically react with the amine group (—NH_2) of the APTES precursor. The chemical structure of the hybrid molecules was characterized by FTIR, as illustrated in Fig. 1 for the silane–CHC (CA) sample. The presence of C=O is seen from the stretching band near 1720 cm^{-1} and a peak near 1200 cm^{-1} is assigned to the CO single bond. The band at 1000–1200 cm^{-1} became broader in the hybrid spectrum than in that of native CHC, which is believed due to the absorption of Si—O—Si (stretching mode) overlapped with the —C—O—C— glycosidic linkage of the CHC (Bermudez, Carlos, & Alcacer, 1999; Fu et al., 2004; Mahapatro et al., 2006). Together with the absence of the peak at 1720 cm^{-1}, it gave supporting evidence that the carboxylic acid of CHC was replaced by the amine group of APTES. The NH peaks at 1590–1560 cm^{-1} and CO peaks at 1652–1633 cm^{-1} were shifted in the silane–CHC (CA) hybrid. The peak at 900–950 cm^{-1} in the hybrids, indicated a Si—OH stretching mode, suggesting incomplete polycondensation of the silanol groups. In other words, the chemical evolution of the silane along the resulting hybrid backbone resulted in a mixture of a polymeric Si—O—Si network structure together with a certain amount of Si—OH groups, not undergoing further condensation. This also implies limited growth of the polymeric silane network along the hybrid chain.

3.2. NMR analysis

Fig. 2a (Table S1) shows the ^{13}C solid-state NMR spectra of neat CHC and the silane–CHC (CA) hybrid. For the hybrids, the linkage of the silane to the CHC polymer is confirmed by the appearance of new signals at ca. 11, 23, 44 and 160–170 ppm. The peaks located at about 11, 23, and 43 ppm are characteristic peaks of the $(CH_2)_3$ aliphatic chains and the ester group carbons bonded to silicon atoms (—Si—CH_2CH_3). The peak at around 164 ppm is suggested to originate from a de-shielded ^{13}C (C=O group), in an electron-withdrawing amide environment which is clearly evidenced in all the spectra as also reported in literature (Franville, Mahiou, Zambon, & Cousseins, 2001; Fu et al., 2004; Goncalves et al., 2004). This observation, together with aforementioned IR analysis, strongly supports the chemical linkage of silane group with the organic CHC macromolecule through the carbodiimide coupling reaction, where the carboxylic acid of the CHC was chemically coupled with the —NH_2 group of APTES.

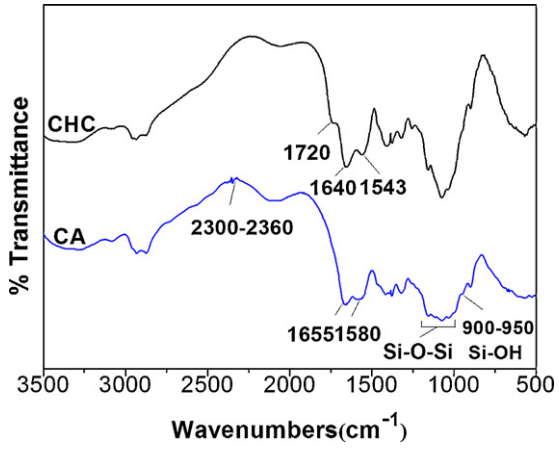

Fig. 1. FTIR spectra of CHC and silane–CHC hybrid (CA).

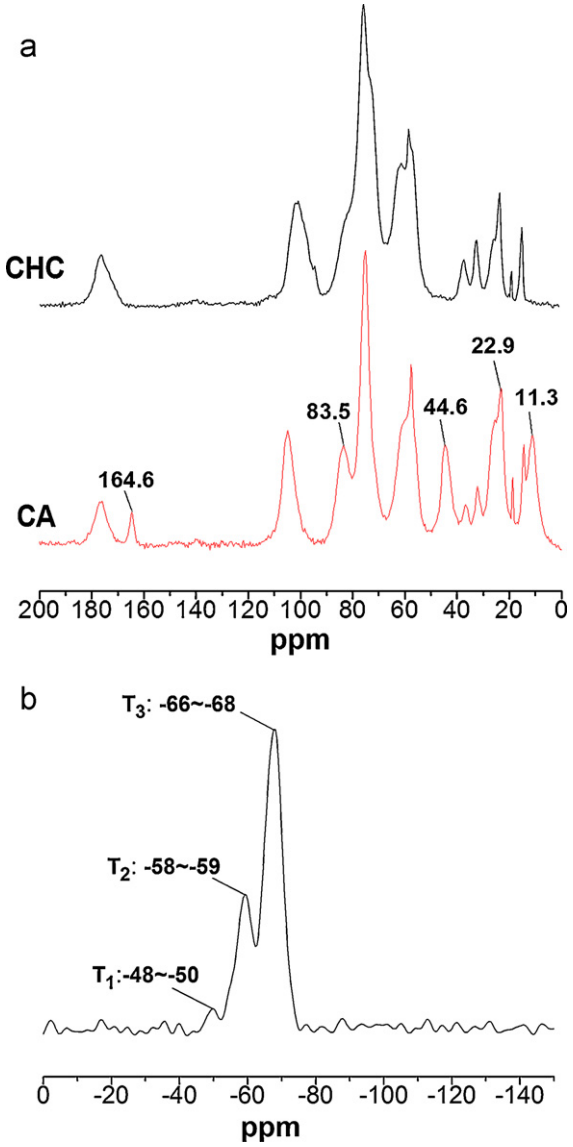

Fig. 2. (a) ^{13}C solid state NMR spectra of CHC and silane–CHC hybrid (CA). (b) ^{29}Si solid state NMR spectra of silane–CHC hybrid.

The potential structural evolution of APTES, once chemically anchored along the hybrid chain, was further examined through ^{29}Si solid state NMR spectra of the hybrid. As seen in Fig. 2b (Table S2), the hybrid spectrum exhibits characteristic signals of T_1 (−48 to −50 ppm), T_2 (−58 to −59 ppm) and T_3 (−66 to −68 ppm), as expected from literature (Carlos, Ferreira, Orion, Bermudez, & Rocha, 2000; Fu et al., 2004; Silva et al., 2005). These sites are labelled using the conventional T_n notation, where n (n = 1, 2, 3) is

the number of Si-bridging oxygen atoms, which represents the –Si in different environments. The spectra indicated that the hybrids were dominated with the T_2 and T_3 environments (at −59 and −68 ppm, respectively) indicating the presence of two main types of local structures: $(SiO)_2Si(CH_2)_3OH$ and $(SiO)_3Si(CH_2)_3$, respectively. The small peak at ca. −48 ppm is ascribed to T_1 sites, and is translated as $(SiO)Si(CH_2)_3(OH)_2$ structure. Therefore, it is clear that the silane chemically attached with the CHC chain is virtually a mixture of a small amount of Si—OH and a large quantity of Si—O—Si groups. From the T_2 and T_3 structures of the ^{29}Si-NMR spectra, it is reasonable to conclude that the silane groups (Si—OH) were subsequently condensed to form a Si—O—Si network. We therefore postulate that once the condensation occurred, a certain population of APTESs formed an internal Si—O—Si network, while some residual silanol (incomplete condensation) groups remained organized towards the aqueous environment, the prevalence of Si—O—Si groups increased, on the expense of Si—OH, with increasing Si:CHC ratio used during synthesis (see Supplementary Material). This was later found to play a critical role in the self-assembly and resulting size of the nanoparticles.

3.3. Structural evolution of the hybrid nanoparticles

From the spectroscopic analyses, the molecular structure of resulting hybrids can be proposed as schematically illustrated in Fig. 3, where the silane group was covalently bridged to the carboxylic acid of the CHC, forming both Si—OH and Si—O—Si groups along the CHC chain, while the hydrophobic hexanoyl groups of the hybrid molecules remained intact. Accordingly, such a hydrophobic–hydrophilic arrangement along the backbone of hybrid molecule imparts a self-assembly potential when the hybrid molecules are exposed to an aqueous medium (Li, Zhuang, Mu, Wang, & Fang, 2008; Liu, Xu, Guo, & Han, 2009; Sun et al., 2009; Wang, Liu, Weng, & Zhang, 2007; Zhu, Chan-Park, Dai, & Li, 2005) potentially forming a thermodynamically stable nanoparticle in order to minimize the free energy of the solution system. To confirm this hypothesis the silane–CHC hybrid molecules were dissolved in DI water and the morphology was subsequently analysed using SEM and TEM. The SEM analysis revealed that the hybrid molecules indeed self-assembled into nanoparticles, displaying a sphere-like appearance with an average size of about 60 nm in diameter (Fig. 4(a)). However, a closer look at these nanoparticles revealed a seemingly polygonal morphology, rather than a perfect sphere (inset in Fig. 4(a)). This finding indicates that the incorporation of the silane nanophase alters the morphological development of the hybrid nanoparticles.

The hybrid nanoparticles show a typically broad silane X-ray diffraction peak at around 20–30° (inset in Fig. 4(a)) after self-assembly in water, indicating an amorphous nature of the silane formed in the hybrid. TEM analysis revealed that the silane formed a layer-like morphology of ~6 nm in width around the nanoparticles (Fig. 4(b)). Since the silane phase was confirmed as the inorganic constituent of the resulting hybrid molecules, the silane layer should then be built up as a result of natural assembly of the hybrid molecules in water. Furthermore, high-resolution TEM examination, inset photo in Fig. 4(b), revealed orderly arranged silane lattices, indicating that such an assembly should be self-organized, rather than randomly aggregated. However, this tiny crystalline silane lattice probably did not give a sharp X-ray diffraction pattern (inset of Fig. 4(a)) due to the lack of long-range regularity. The self-organized arrangement of the silane nano-phases also suggests that the hybrid molecules aggregated to a certain extent in an organized manner. After a closer look at the morphological development of the silane nano-phases in Fig. 4(b), we found the presence of some sharp corners in the inner layers, i.e. an angle of about 90°, rather than the highly curved shape of the hybrid nanoparticles' surfaces. One plausible explanation for this difference may be that the hybrid molecules are assembled into a highly curved geometry around the sharp cornered silane layers of the inner most regions of the nanoparticles, during the assembly differences in atomic packing arrangement from inside to outside of the highly curved shape may cause lattice mismatch in packing configuration, giving rise to

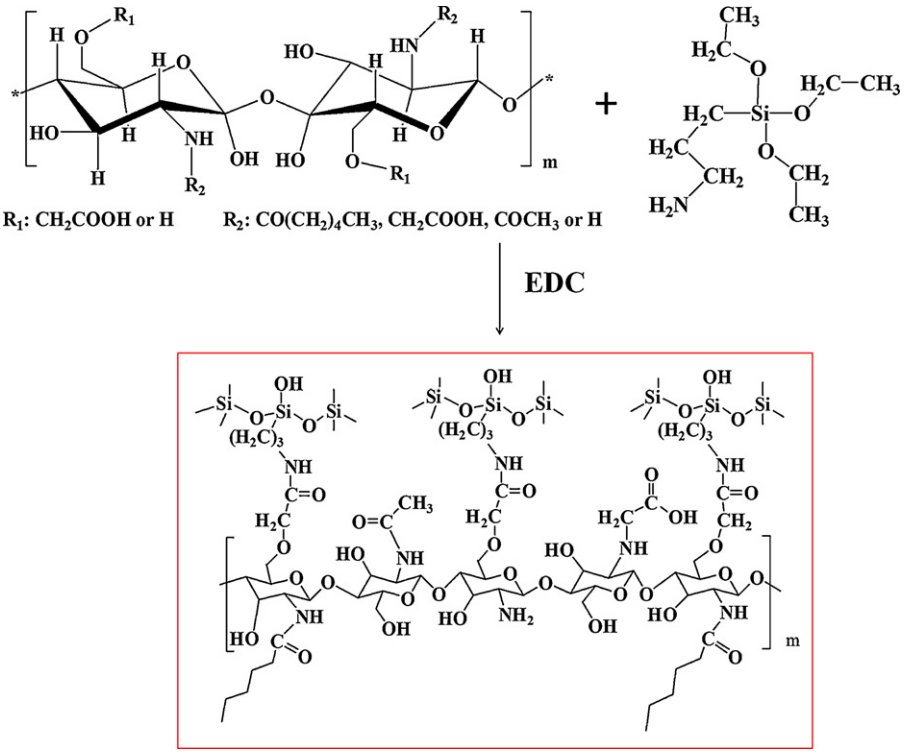

Fig. 3. Proposed molecular structure of the hybrid molecules synthesized in this work.

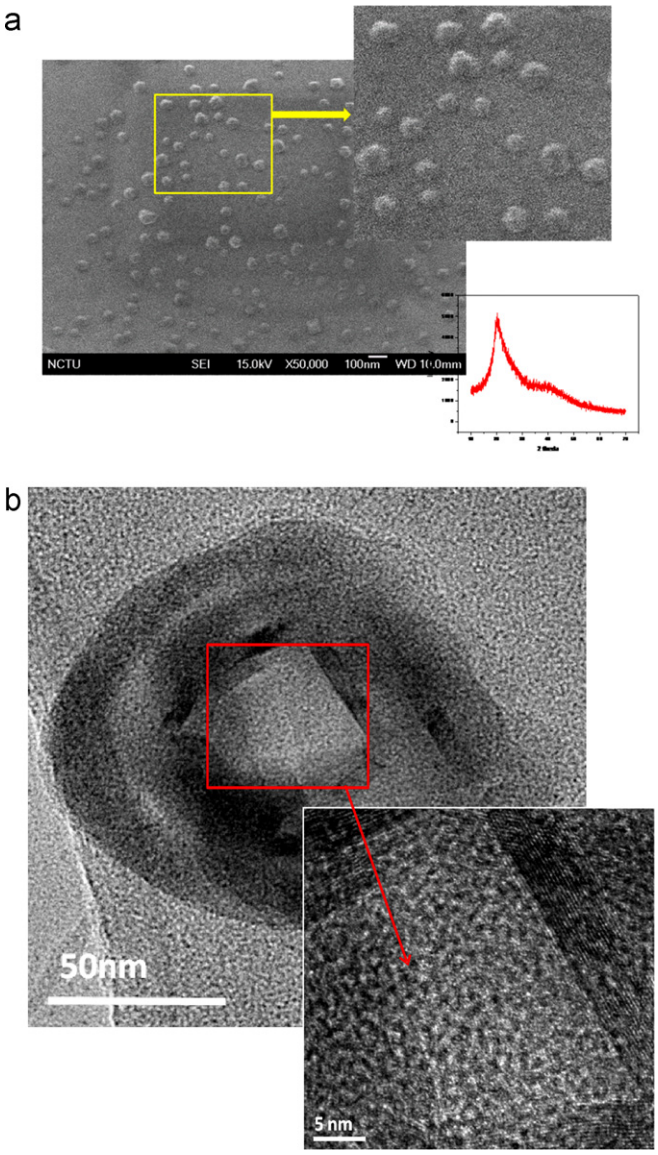

Fig. 4. (a) SEM image of silane–CHC hybrid nanoparticles, where the size of the nanoparticles is about 65 nm in average. The nanoparticles exhibit a polygonal geometry, rather than perfect sphere (inset) and also show an amorphous X-ray diffraction pattern (inset). (b) TEM image of the silane–CHC hybrid nanoparticle, the resulting nanoparticle displays a layer-like silane nanophase of about 6 nm in thickness surrounding the nanoparticle, where (inset) a high resolution TEM image further shows the crystalline arrangement of the silane layer.

stress development and thus to the polygonal structures observed, see Fig. 4(a).

3.4. Self-assembly behaviour

The self assembly potential of amphiphilic chitosan into nanoparticles is reported previously (Liu et al., 2009; Wang et al., 2007), an important parameter to characterize for such self-assembling systems is the critical aggregation concentration (CAC). Pyrene is frequently used as a fluorescence probe to investigate the self-aggregation behaviour of amphiphilic polymers at a molecular level (Amiji, 1995; Lee, Jo, Kwon, Kim, & Jeong, 1998; Wilhelm et al., 1991). Thus the CAC was determined by measuring the variation of the spectral emission peak ratio I_{372}/I_{385} value for pyrene in the presence of silane–CHC at different concentrations. Fig. 5(a) illustrates the variation of I_{372}/I_{385} ratio of pyrene as a function of the concentration of the hybrids with various —COOH-to-NH_2

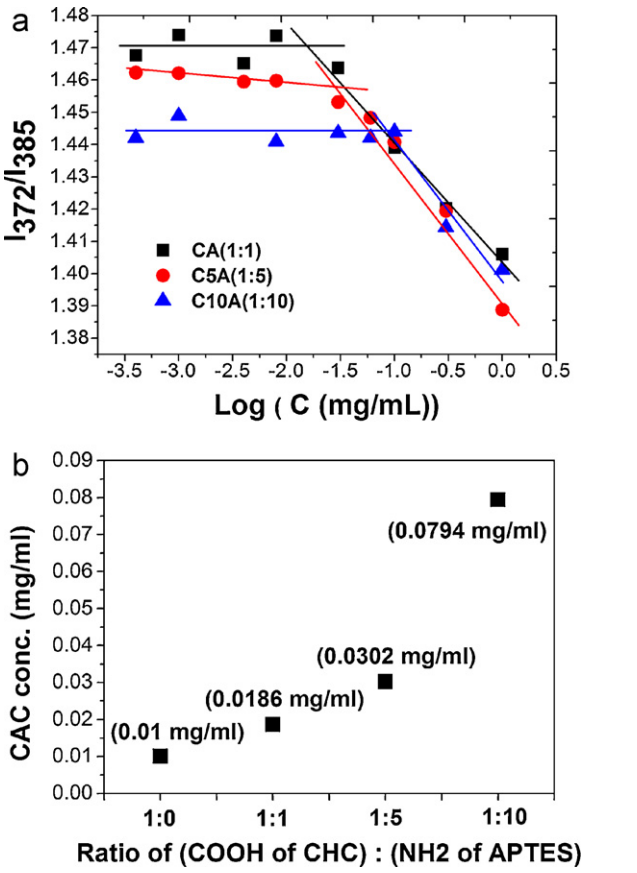

Fig. 5. (a) The variation of I_{372}/I_{385} of pyrene with the concentration for hybrid molecules with various CHC:APTES ratios. The intersect of the straight lines indicates the abrupt change in I_{372}/I_{385}, associated with the CAC, for the different compositions. (b) The critical aggregation concentration (CAC) for hybrid molecules with different ratios of CHC:APTES.

ratios. The CAC for each composition was then determined from the intersection of the two linear regions.

As shown in Fig. 5(b) and Table 1, and compared with neat amphiphilic CHC, a higher CAC value was always obtained, i.e., the lowest CAC was 0.0186 mg/ml for 1:1 composition, compared with 0.01 mg/ml for neat CHC. This increase in CAC with increasing amount of silane reacted onto the CHC (confirmed by NMR) suggesting that the self-assembly behaviour was altered depending on the silane content of the hybrid molecules, in line with DLS results discussed above. The mechanism of the increase in CAC with increasing silane content can be explained by the increase in Si—O—Si groups and decrease in Si—OH groups, discussed above. The changed chemistry of the hybrid molecules may alter the hydrophobic–hydrophilic interaction originally present in the CHC molecules in aqueous environment, thus changing the self-assembly behaviour. Moreover, the Si—O—Si network, may also modify the self-assembly behaviour of the hybrid molecules due to the bulkiness of such a network.

Table 1
Mean size (by DLS) of hybrid nanoparticles with different ratios of (COOH of CHC):(NH_2 of APTES), ranging from 1:0 (CHC) to 1:10 (C10A).

Sample name	Mean size (nm)
CHC	117.2 ± 14.0
CA	124.8 ± 18.3
C5A	468.4 ± 34.9
C10A	588.5 ± 64.3

We also found that the presence of silane stabilized the resulting hybrid nanoparticles from undesirable structural disintegration when the concentration is largely diluted (>10 times) below the CAC, i.e., samples prepared for TEM examination, without any cross-linkers used. Such a structural stabilization may be derived from a consecutive condensation reaction among the silanol groups between hybrid molecules, joined together as a result of assembly, forming Si—O—Si links, resulting in irreversible cross-links in the resulting hybrid nanoparticles.

3.5. Drug loading and release from the hybrid nanoparticles

Drug encapsulation and release behaviour of hybrid nanoparticles were investigated using (S)-(+)-camptothecin (CPT) as model molecule. The drug loading efficiency was evaluated for silane–CHC hybrid molecules by adding various concentrations ranging from 0.5 mg/ml to 9 mg/ml, to a water DMSO solution containing the drug at a concentration of 50 μg/mL. Fig. 6(a) shows that the loading efficiency was dependent on the concentration of the hybrid molecules, where a decrease in loading efficiency was observed with increasing hybrid concentration. The loading efficiency decreased from 92% to 68% when the hybrid concentration was increased from 0.5 mg/ml to 9 mg/ml. The decrease in loading efficiency with increasing polymer concentration has been previously reported for chitosan based nano-microcapsule systems

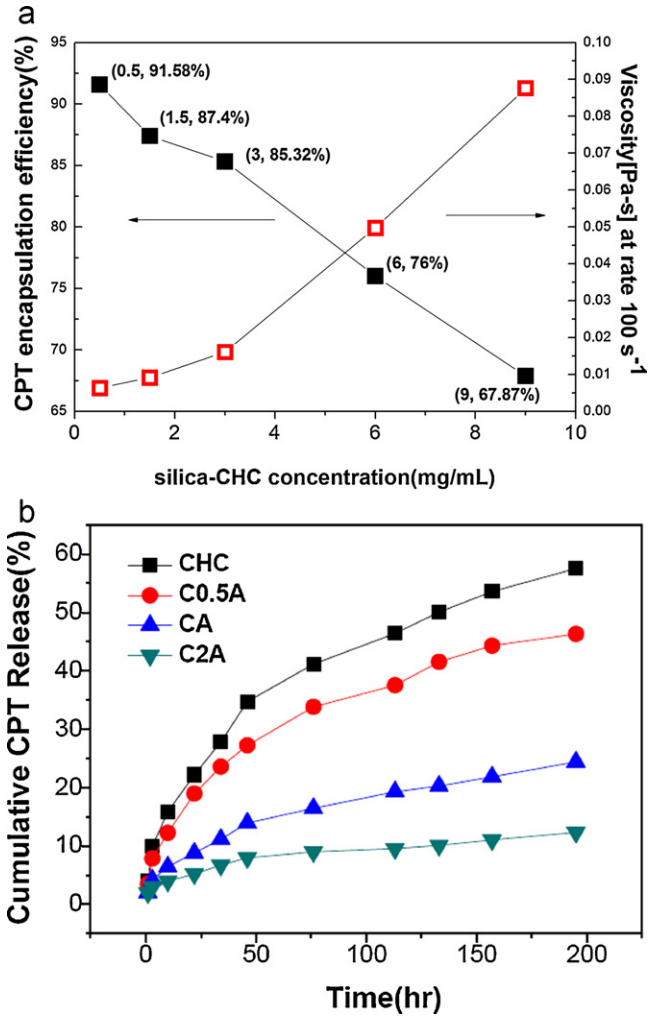

Fig. 6. (a) The concentration-dependent CPT loading efficiency and the corresponding viscosity of the solution for silane–CHC hybrid molecules. (b) The CPT release profile from pure CHC and hybrid nanoparticles with different CHC:APTES ratios.

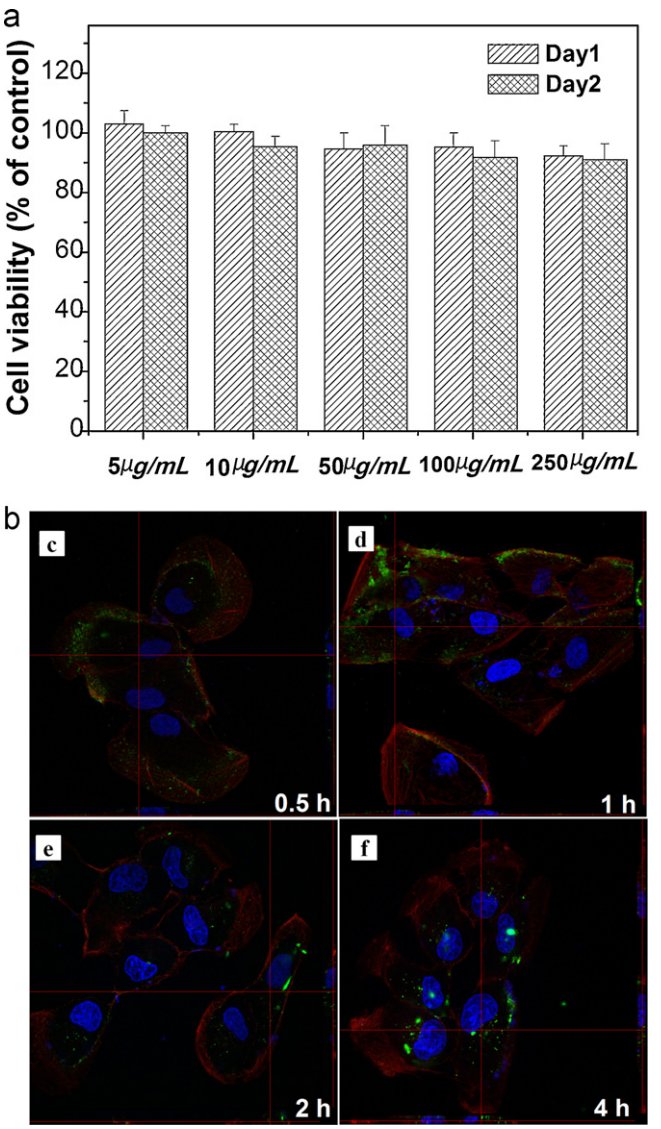

Fig. 7. (a) Cell viability of ARPE-19 cells after 1 and 2 days of incubation with various concentrations of silane–CHC hybrid nanoparticles. (b) Time-course confocal microscopy images of ARPE-19 cells labelled with FITC-silane–CHC hybrid nanoparticles, the cell skeleton was stained with rhodamine phalloidin (red), cell nucleus with DAPI (blue). Cells were incubated with FITC-silane–CHC hybrid nanoparticles for (c) 30 min, (d) 1 h, (e) 2 h and (f) 4 h. (For interpretation of the references to color in this figure legend, the reader is referred to the web version of this article.)

(Vandenberg, Drolet, Scott, & de la Noue, 2001; Zhang, Wu, Tao, Zang, & Su, 2010; Zheng et al., 2011; Zhu, Chen, Yuan, Wu, & Lu, 2006). This concentration-dependent drug loading efficiency may be explained in two ways: (1) the solution viscosity increases with increasing hybrid molecule concentration and (2) with increasing hybrid molecule concentration there is a change in aggregate structure that causes the silane–CHC aggregates to encapsulate drug less efficiently. For the former, the increased solution viscosity, as illustrated in Fig. 6(a), may kinetically retard the self-assembly rate of the hybrid molecules. This argument is supported by an excellent correlation (R^2 as high as 0.98) between solution viscosity and encapsulation efficiency. The solution with increased viscosity should hinder, to a certain extent, molecular mobility upon the course of assembly. To this point, we may conclude that the slower the self-assembly rate, due to higher solution viscosity, the poorer encapsulation efficiency. However, despite a concentration-dependent drug loading efficiency, it is encouraging that promising

encapsulation efficiency, greater than 90%, was achieved under optimal encapsulation conditions.

Fig. 6(b) shows the release profiles of CPT from hybrid nanoparticles prepared using different Si:CHC ratios, neat CHC is included for comparison. CPT released from the hybrid nanoparticles occurred at a slower rate than from CHC, the drug release was slightly slower for C0.5A nanocapsules, but dramatically decreased for CA and C2A nanocapsules. This finding suggests a dominating effect of the silane layer above a threshold silane content. The silane layer seems to act as an effective physical barrier, even with a thickness of only about 6 nm, preventing the CPT to diffuse out from the particles.

3.6. Cytocompatibility and cellular uptake

The cytotoxicity of the hybrid nanoparticles against human retinal pigmented epithelium cell (ARPE-19) is given in Fig. 7(a). The cytotoxicity increased slightly with added concentration of nanoparticles and incubation time. However, the cell viability remained as high as 88% for the sample with the highest nanoparticle concentration (250 μg/mL) after 48 h of incubation, indicating an excellent cytocompatibility with respect to the human retinal pigmented epithelium cells.

In Fig. 7(b) the cellular uptake of the FITC-labelled hybrid nanoparticles, over an incubation period from 0.5 h to 4 h, is shown. The hybrid nanoparticles were gradually absorbed by the cells; in the first 0.5 h, only a few green spots were detected along the cell surface, indicating that the FITC-labelled hybrids attached to the surface of the cell membranes. After 1 h incubation, some of the hybrid nanoparticles appeared to enter into the cytoplasm region of the cells and more hybrid nanoparticles attached to the membrane region. At 4 h a considerable amount of the hybrid nanoparticles was internalized into cytoplasm region. Although the detailed mechanism of endocytosis of the hybrid nanoparticles is unclear at present, this observation suggests that the newly developed hybrid nanoparticles are not only biocompatible, but are capable of internalizing in an efficient manner for the cell line under investigation. The cells, after internalization of large amount of the hybrid nanoparticles for over 48 h, showed little change in cell geometry, i.e. size and shape, indicating a negligibly detrimental effect of the hybrid nanoparticles. Both the low cytotoxicity and the promising absorption of the hybrid nanoparticles strengthen the potential to use the hybrid nanoparticles as drug delivery vehicles.

4. Conclusion

A novel hybrid macromolecule based on a chemical modification along the —COOH groups of amphiphilic chitosan (CHC) with (3-aminopropyl)triethoxysilane molecules was successfully synthesized. The hybrid molecule showed a concentration-dependent self-assembly behaviour making a final hybrid nanoparticle tuneable in size, drug encapsulation efficiency and release profile. Formation of a highly ordered silane layer of ~6 nm in thickness, upon self-assembly of the hybrid molecule leads to a sustained release of the model drug, CPT, compared with pure CHC molecules. The thin silane layer formed within the hybrid nanoparticles provided not only a well-stabilized nanostructure without the need of crosslinker, but proved to be a highly self-organized, rather than random, arrangement of the hybrid macromolecules. The hybrid molecules demonstrated efficient cellular internalization and excellent cytocompatibility to human retinal pigmented epithelium cell (ARPE-19). These observations strongly suggest a potential use of the developed amphiphilic hybrid macromolecules in biomedical applications, especially as drug delivery vehicles.

Acknowledgements

The authors want to express their sincere gratitude to Mikael Larsson at Chemical and Biological Engineering, Chalmers University of Technology for valuable discussions and assistance in the preparation of the manuscript. Furthermore, the authors would like to give their thanks to the National Science Council, Taiwan, Republic of China, for a financial support under a project contract of NSC-99-2113-M-009-004.

Appendix A. Supplementary data

Supplementary data associated with this article can be found, in the online version, at http://dx.doi.org/10.1016/j.carbpol.2012.03.066.

References

Amiji, M. M. (1995). Pyrene fluorescence study of chitosan self-association in aqueous-solution. *Carbohydrate Polymers*, *26*(3), 211–213.

Bermudez, V. D., Carlos, L. D., & Alcacer, L. (1999). Sol–gel derived urea cross-linked organically modified silicates. 1. Room temperature mid-infrared spectra. *Chemistry of Materials*, *11*(3), 569–580.

Carlos, L. D., Ferreira, R. A. S., Orion, I., Bermudez, V. D., & Rocha, J. (2000). Sol–gel derived nanocomposite hybrids for full colour displays. *Journal of Luminescence*, *87-89*, 702–705.

Franville, A. C., Mahiou, R., Zambon, D., & Cousseins, J. C. (2001). Molecular design of luminescent organic–inorganic hybrid materials activated by europium (III) ions. *Solid State Sciences*, *3*(1–2), 211–222.

Fu, L. S., Ferreira, R. A. S., Silva, N. J. O., Carlos, L. D., Bermudez, V. D., & Rocha, J. (2004). Photoluminescence and quantum yields of urea and urethane cross-linked nanohybrids derived from carboxylic acid solvolysis. *Chemistry of Materials*, *16*(8), 1507–1516.

Gamys, C. G., Beyou, E., & Bourgeat-Lam, E. (2010). Micellar behavior of well-defined polystyrene-based block copolymers with triethoxysilyl reactive groups and their hydrolysis–condensation. *Journal of Polymer Science Part A: Polymer Chemistry*, *48*(4), 784–793.

Goncalves, M. C., Bermudez, V. D., Ferreira, R. A. S., Carlos, L. D., Ostrovskii, D., & Rocha, J. (2004). Optically functional di-urethanesil nanohybrids containing Eu^{3+} ions. *Chemistry of Materials*, *16*(13), 2530–2543.

Guo, X. H., Zheng, D., & Hu, N. F. (2008). Enhancement of Au nanoparticles formed by in situ electrodeposition on direct electrochemistry of myoglobin loaded into layer-by-layer films of chitosan and silica nanoparticles. *Journal of Physical Chemistry B*, *112*(48), 15513–15520.

Hu, F. Q., Liu, L. N., Du, Y. Z., & Yuan, H. (2009). Synthesis and antitumor activity of doxorubicin conjugated stearic acid-g-chitosan oligosaccharide polymeric micelles. *Biomaterials*, *30*(36), 6955–6963.

Jayakumar, R., Chennazhi, K. P., Muzzarelli, R. A. A., Tamura, H., Nair, S. V., & Selvamurugan, N. (2010). Chitosan conjugated DNA nanoparticles in gene therapy. *Carbohydrate Polymers*, *79*(1), 1–8.

Lee, K. Y., Jo, W. H., Kwon, I. C., Kim, Y. H., & Jeong, S. Y. (1998). Physicochemical characteristics of self-aggregates of hydrophobically modified chitosans. *Langmuir*, *14*(9), 2329–2332.

Lei, L. H., Cao, Z. J., Xie, Q. J., Fu, Y. C., Tan, Y. M., Ma, M., et al. (2011). One-pot electrodeposition of 3-aminopropyltriethoxysilane–chitosan hybrid gel film to immobilize glucose oxidase for biosensing. *Sensors and Actuators B-Chemical*, *157*(1), 282–289.

Li, G., Zhuang, Y. L., Mu, Q., Wang, M. Z., & Fang, Y. E. (2008). Preparation, characterization and aggregation behavior of amphiphilic chitosan derivative having poly(L-lactic acid) side chains. *Carbohydrate Polymers*, *72*(1), 60–66.

Liu, K. H., Chen, S. Y., Liu, D. M., & Liu, T. Y. (2008). Self-assembled hollow nanocapsule from amphiphatic carboxymethyl-hexanoyl chitosan as drug carrier. *Macromolecules*, *41*(17), 6511–6516.

Liu, L., Xu, X., Guo, S. A. R., & Han, W. (2009). Synthesis and self-assembly of chitosan-based copolymer with a pair of hydrophobic/hydrophilic grafts of polycaprolactone and poly(ethylene glycol). *Carbohydrate Polymers*, *75*(3), 401–407.

Mahapatro, A., Johnson, D. M., Patel, D. N., Feldman, M. D., Ayon, A. A., & Agrawal, C. M. (2006). Surface modification of functional self-assembled monolayers on 316L stainless steel via lipase catalysis. *Langmuir*, *22*(3), 901–905.

Mullner, M., Schallon, A., Walther, A., Freitag, R., & Muller, A. H. E. (2010). Clickable, biocompatible, and fluorescent hybrid nanoparticles for intracellular delivery and optical imaging. *Biomacromolecules*, *11*(2), 390–396.

Murakami, K., Aoki, H., Nakamura, S., Nakamura, S., Takikawa, M., Hanzawa, M., et al. (2010). Hydrogel blends of chitin/chitosan, fucoidan and alginate as healing-impaired wound dressings. *Biomaterials*, *31*(1), 83–90.

Muzzarelli, R. A. A. (1993). Biochemical significance of exogenous chitins and chitosans in animals and patients. *Carbohydrate Polymers*, *20*(1), 7–16.

Muzzarelli, R. A. A. (2009). Chitins and chitosans for the repair of wounded skin, nerve, cartilage and bone. *Carbohydrate Polymers*, *76*(2), 167–182.

Qi, X. Y., Xue, C., Huang, X., Huang, Y. Z., Zhou, X. Z., Li, H., et al. (2010). Polyphenylene dendrimer-templated in situ construction of inorganic–organic hybrid rice-shaped architectures. *Advanced Functional Materials*, *20*(1), 43–49.

Salmah, H., Faisal, A., & Kamarudin, H. (2011). Chemical modification of chitosan-filled polypropylene (PP) composites: The effect of 3-aminopropyltriethoxysilane on mechanical and thermal properties. *International Journal of Polymeric Materials*, *60*(7), 429–440.

Silva, S. S., Ferreira, R. A. S., Fu, L. S., Carlos, L. D., Mano, J. F., Reis, R. L., et al. (2005). Functional nanostructured chitosan–siloxane hybrids. *Journal of Materials Chemistry*, *15*(35-36), 3952–3961.

Sun, Z. C., Bai, F., Wu, H. M., Schmitt, S. K., Boye, D. M., & Fan, H. Y. (2009). Hydrogen-bonding-assisted self-assembly: Monodisperse hollow nanoparticles made easy. *Journal of the American Chemical Society*, *131*(38), 13594–13595.

Tripathi, B. P., & Shahi, V. K. (2008). Functionalized organic–inorganic nanostructured N-p-carboxy benzyl chitosan–silica–PVA hybrid polyelectrolyte complex as proton exchange membrane for DMFC applications. *Journal of Physical Chemistry B*, *112*(49), 15678–15690.

Vandenberg, G. W., Drolet, C., Scott, S. L., & de la Noue, J. (2001). Factors affecting protein release from alginate–chitosan coacervate microcapsules during production and gastric/intestinal simulation. *Journal of Controlled Release*, *77*(3), 297–307.

Wang, G. H., & Zhang, L. M. (2006). Using novel polysaccharide–silica hybrid material to construct an amperometric biosensor for hydrogen peroxide. *Journal of Physical Chemistry B*, *110*(49), 24864–24868.

Wang, Y. S., Liu, L. R., Weng, J., & Zhang, Q. Q. (2007). Preparation and characterization of self-aggregated nanoparticles of cholesterol-modified O-carboxymethyl chitosan conjugates. *Carbohydrate Polymers*, *69*(3), 597–606.

Wen, J. Y., & Wilkes, G. L. (1996). Organic/inorganic hybrid network materials by the sol–gel approach. *Chemistry of Materials*, *8*(8), 1667–1681.

Wilhelm, M., Zhao, C. L., Wang, Y. C., Xu, R. L., Winnik, M. A., Mura, J. L., et al. (1991). Polymer micelle formation. 3. Poly(styrene-ethylene oxide) block copolymer micelle formation in water – A fluorescence probe study. *Macromolecules*, *24*(5), 1033–1040.

Yavuz, M. S., Cheng, Y. Y., Chen, J. Y., Cobley, C. M., Zhang, Q., Rycenga, M., et al. (2009). Gold nanocages covered by smart polymers for controlled release with near-infrared light. *Nature Materials*, *8*(12), 935–939.

Zhang, H. L., Wu, S. H., Tao, Y., Zang, L. Q., & Su, Z. Q. (2010). Preparation and characterization of water-soluble chitosan nanoparticles as protein delivery system. *Journal of Nanomaterials*,

Zheng, H., Zhang, X. Q., Xiong, F. L., Zhu, Z. J., Lu, B., Yin, Y. H., et al. (2011). Preparation, characterization, and tissue distribution in mice of lactosaminated carboxymethyl chitosan nanoparticles. *Carbohydrate Polymers*, *83*(3), 1139–1145.

Zhu, A. P., Chan-Park, M. B., Dai, S., & Li, L. (2005). The aggregation behavior of O-carboxymethylchitosan in dilute aqueous solution. *Colloids and Surfaces B: Biointerfaces*, *43*(3–4), 143–149.

Zhu, A. P., Chen, T., Yuan, L. H., Wu, H., & Lu, P. (2006). Synthesis and characterization of N-succinyl–chitosan and its self-assembly of nanospheres. *Carbohydrate Polymers*, *66*(2), 274–279.